

Investigation on the photocatalytic behaviors of europium carbonate and oxide nanoparticles prepared based on statistically optimized carbonation and calcination routes

Mehdi Rahimi-Nasrabadi^{1,2}  · Seied Mahdi Pourmortazavi³ ·
Meisam Sadeghpour Karimi⁴ · Mustafa Aghazadeh⁵ · Mohammad Reza Ganjali^{4,6} ·
Parviz Norouzi^{4,6}

Received: 12 March 2017 / Accepted: 15 May 2017 / Published online: 22 May 2017
© Springer Science+Business Media New York 2017

Abstract This study is focused on evaluating the photocatalytic properties of the europium carbonate and oxide nanoparticles synthesized via optimizing the direct precipitation and decomposition of the precipitate as a precursor into europium oxide by thermal decomposition. The emphasis was directed towards determining the optimal reaction conditions. To this end, the Taguchi method was used to determine the best parameters for the reaction. The carbonate product at this stage, was used in a further step where it underwent a one-step calcinations treatment leading to its decomposition into europium oxide nanoparticles. The nanoparticles were next characterized using X-ray diffraction, SEM, FT-IR and thermal analysis techniques. Then, the photocatalytic behaviors of the europium carbonate and oxide nanoparticles for the photocatalytic degradation of methyl orange under ultraviolet light was

investigated and the results exhibited efficient degradation of the target in the presence of both nanoparticles as photocatalysts.

1 Introduction

Environmental problems are among the major concerns of humans in the modern era. Along with the expansion of industries, environmental pollution and infection around us has increased quickly [1–5]. Therefore, decontamination of water and infection control procedures have a great importance and in recent year's extensive research has been done in this area and various methods have been invented. Among the various methods photocatalysts according to their unique features have created great promise in this regard [6–8].

Compounds of rare earth elements have extensive applications in high performance luminescence devices, catalysts and other functional materials due to their unique electronic, optical and chemical properties, which root in their 4f electrons [9, 10]. The luminescence of Eu^{3+} has its the main emission band at around 611 nm (red), which is a primary color and hence Eu^{3+} has been evaluated as a luminescence activator in many host lattices [11, 12].

Further to its intense red emission, the ion's luminescence spectra includes rather narrow bands, which can be used as effective luminescent sources [13, 14]. Additionally, the interpretation of the spectral data on Eu^{3+} is interesting, since the ion has the advantage of having non-degenerate ground and emitting states. Hence the ${}^5\text{D}_0 \rightarrow {}^7\text{F}_0$ transition can yield purity or site symmetry information, plus being suitable for the study of transition probabilities on the sharp spectral features in lanthanides [15].

✉ Mehdi Rahimi-Nasrabadi
rahiminasrabadi@gmail.com; kpmrahimi@ihu.ac.ir

✉ Seied Mahdi Pourmortazavi
poumortazavi@yahoo.com

¹ Faculty of Pharmacy, Baqiyatallah University of Medical Sciences, Tehran, Iran

² Department of Chemistry, Imam Hossein University, Tehran, Iran

³ Faculty of Material and Manufacturing Technologies, Malek Ashtar University of Technology, Tehran, Iran

⁴ Center of Excellence in Electrochemistry, University of Tehran, Tehran, Iran

⁵ Nuclear Science and Technology Research Institute (NSTRI), P.O. Box 14395-834, Tehran, Iran

⁶ Biosensor Research Centre, Endocrinology & Metabolism Molecular and Cellular Research Institute, Tehran University of Medical Sciences, Tehran, Iran

Eu_2O_3 is a very important oxide phosphor, which is well known for light emissivity and electrical insulating properties [15] and considered a possible candidate for high k-gate dielectrics for transistor applications [16]. Consequently the application of Eu_2O_3 as a luminescence activator, in several host lattices has been the subject of scientific scrutiny [17]. Nanocomposites of europium hydroxide or oxide with CNT have also been prepared recently [18, 19].

Europium is one of the lanthanide ions that can be used in photocatalyst compounds [10]. It has been shown that the photocatalytic activity of TiO_2 nanoparticles doped with lanthanide ions, increases in the degradation of methyl orange dye [20]. It could be considered evident that the combination of these properties with those of nanoparticles, which have shown a great potential for use in optics, heterogeneous catalysis, photocatalyst and magnetics [21], coatings or thin films. The compounds can lead to large improvements in the fabrication of optical devices like optical amplifiers and microlasers in submicron scales [22]. To this end the synthesis of rare earth based nanoparticles and their integration with substrates of desire, such as single crystals, ceramic microspheres or nanofibres is necessary.

So far, various techniques, including sonochemical [23], colloidal chemical [24], solvothermal [25], hydrothermal [26] and precipitation [27] techniques, have been used to prepare various europium compounds. Nonetheless, owing to the widespread applications of europium oxide nanoparticles, gaining control over the synthesis of the compounds, through cost effective methods leading to desired morphology, is considered valuable and hence this work was aimed at optimizing the chemical precipitation method for the preparation of high-purity europium carbonate nanoparticles, through using the reaction between $\text{EuCl}_3 \cdot 6\text{H}_2\text{O}$ and Na_2CO_3 solutions. The effects of the different parameters (i.e. the concentrations of europium ion and carbonate solutions, flow rate of addition of the reactants as well as the reactor temperature) were optimized through an experimental design procedure to yield the products of desired dimensions. Later a thermal decomposition stage was performed on the product of the first stage as a precursor. The thermal decomposition reaction was monitored through thermal analysis studies, which make it possible to monitor weight changes throughout the thermal experiments due to dehydration or decomposition. The outcome of the studies was used to provide the data required for optimizing the decomposition reaction leading to the formation of nanoscale crystals of europium oxide. UV–Vis diffuse reflectance spectroscopy (DRS) was used to explore the band gap energy of the nanoparticles products, while, the photo-catalytic behaviors of the nanoparticles in eliminating MO from water samples, was evaluated.

2 Experimental

2.1 Materials and apparatus

Reagent-grade europium chloride, sodium carbonate and ethanol, were procured from Merck Co. and used as received. Scanning electron micrographs (SEMs) were acquired using a Philips XL30 series instrument with a gold film (prepared by a Sputter Coater model SCD005 made by BAL-TEC (Switzerland)) for loading the dried particles onto the instrument. Transmission electron microscopy (TEM) images were obtained using a Zeiss- EM900 scanning electron microscope.

The sample preparation, was performed by loading the sample on a Cu-carbon coated grid. The XRD spectra of the samples were acquired using a Rigaku D/max 2500 V diffractometer equipped with a graphite monochromator and a Cu target. The IR spectra were recorded using a Bruck Equinox 55 IR spectrophotometer through the KBr pellet method. Thermogravimetry (TG) and differential thermal analyses (DTA) were performed on a Stanton Redcroft, STA-780 series with an aluminum crucible. The heating rate during the experiments was $10\text{ }^\circ\text{C}/\text{min}$ in a temperature range of $20\text{--}800\text{ }^\circ\text{C}$ while purging nitrogen at a flow rate of $50\text{ mL}/\text{min}$. The tests were performed using 5.0 mg samples. The UV–Vis diffuse reflectance spectra (DRS) were recorded under ambient conditions using an Avaspec-2048-TEC spectrometer. The UV–Vis studies on the polluted and treated water samples were performed on a Perkin- Elmer Lambda 25 UV/Vis spectrometer.

2.2 Synthesis of europium(III) carbonate

To produce the europium carbonate(III) nanoparticles, different concentrations of Eu^{3+} were added to carbonate solutions, at various flow rates under strong stirring and at various reactor temperatures. The reaction product was then filtered and washed with distilled water and ethanol three and two times, respectively before drying at $80\text{ }^\circ\text{C}$ for 3 h. The optimization of the reaction parameters was performed by performing an experimental design on the variables (i.e. europium and carbonate concentration, flow rate of feeding europium solution to the carbonate solution, and the reactor temperature) as illustrated in Table 1.

2.3 Thermal decomposition of europium(III) carbonate

Thermal decomposition of europium(III) carbonate at $650\text{ }^\circ\text{C}$ for 2 h was used for the preparation of Eu_2O_3 . This reaction was performed in a furnace under a static air atmosphere. In each experiment, 0.25 g of the precursor

Table 1 OA₉ (3⁴) experimental design and mean particle size of produced europium carbonate as results

Trial number	Eu ³⁺ conc. (mol/L)	CO ₃ ²⁻ conc. (mol/L)	Eu ³⁺ feed flow rate (mL/min)	Temperature (°C)	Diameter of europium carbonate particles (nm)
1	0.01	0.01	2.5	0	37
2	0.01	0.03	10	30	38
3	0.01	0.09	40	60	48
4	0.03	0.01	10	60	41
5	0.03	0.03	40	0	46
6	0.03	0.09	2.5	30	55
7	0.09	0.01	40	30	33
8	0.09	0.03	2.5	60	37
9	0.09	0.09	10	0	47

were loaded into a 30 mm wide and 14 mm height, alumina crucible.

2.4 Diffuse reflectance spectroscopy (DRS)

A technique used to evaluate the optical band gap (OBG) energies of the synthesized europium compounds (i.e. europium carbonate and oxide nanoparticles) is the DRS. OBG energy is defined as the lowest photon energy needed for exciting one electron from the valence band of a semiconductor to its conduction band. Tauc's equation [29]:

$$\alpha h\nu = A(h\nu - E_g)^\eta \quad (1)$$

describes the energy dependence of the absorption edge of a semiconductor. In this equation, h , ν , α , E_g , respectively represent the Planck's constant, frequency of light, absorption coefficient, and band gap energy. A is a constant and η can be either $\frac{1}{2}$ or 2. The $\frac{1}{2}$ value is used for direct transitions, as in the case of europium carbonate and oxide nanoparticles, while 2 is applied in the case of indirect transitions respectively.

2.5 Evaluation of the photocatalytic activities of the nano-structures

The europium carbonate and oxide nanoparticles were used as photocatalysts for the degradation of methyl orange (MO) under UV irradiation. The UV-degradation reactor was a cylindrical Pyrex double pipe air-lift with a high pressure Hg lamp (250 W, $\lambda > 280$ nm) as the UV source. The lamp was lodged in a second quartz pipe co-axially fixed inside the cylindrical Pyrex pipe.

The reaction mixture was a suspension of 0.05 g of the nanoparticles used as the photocatalyst (0.1 g/L) in 500 mL of a solution further containing 5 mg/L of MO.

The mixture was thoroughly stirred in the dark, for 20 min before the reaction was induced through the irradiation. The reaction was run under ultraviolet irradiation and constant aeration, and samples were taken from the mixture after 0, 10, 20, 30, 40 and 50 min. The samples were analyzed on a UV–Vis spectrometry at the λ_{\max} of MO under thermostatic condition at 25 °C, which necessitated cooling the reactor.

Using the Lambert–Beer equation (Eq. 2) [29]:

$$A = \epsilon bC \quad (2)$$

in which A , ϵ , b and C represent the absorbance, molar absorptivity, length of the section of the light path occupied by the sample, and the concentration of the analyte. If A_0 and A_t are the absorbance at 0 and t minutes after the irradiation and C_0 and C_t represent the corresponding concentration of the analyte, we have Eq. 3:

$$\frac{A}{A_0} = \frac{C}{C_0} \quad (3)$$

A_t and A_0 can also be used to calculate the degradation efficiency (DE) of the photocatalyst through Eq. 4:

$$DE (\%) = \frac{A_0 - A_t}{A_0} \times 100 \quad (4)$$

The Langmuir–Hinshelwood model, which is routinely used in the case of photocatalytic degradation of organic molecules at low concentrations, was used to evaluate the kinetics of the degradation of MO by the photocatalysts [28, 29]:

$$-\frac{dC}{dt} = k_{app}C \quad (5)$$

In the above equation C is the concentration of the organic species, k_{app} is the reaction rate constant, and t and $-\frac{dC}{dt}$ are degradation time and reaction rates.

3 Results and discussion

3.1 Results of the precipitation reaction and their optimization through OAD

Precipitation reaction is a common route for the preparation of insoluble salts like europium(III) carbonate [30–32]. However controlling the dimensions of the products of such reactions, is very difficult and involves a complex process which necessitates the fundamental comprehension of the interactions between the effective parameters. In the light of these, we focused on determining how various parameters affect the dimensions of the product particles, through a Taguchi orthogonal array

design [33–35] which is used for the determination of the optimal reaction conditions leading to the best particle size and particle size distribution of the produced europium(III) carbonate. Table 1 illustrates the make-up of the Taguchi's orthogonal array design, as well as the experimental results. The scanning electron microscopy (SEM) images obtained for some europium(III) carbonate samples, prepared by this method, are given in Fig. 1.

Due to orthogonality of the experimental design, averaging the responses at each level can help isolate the effect of each control parameter at different levels. The mean particle size corresponding to each factors, at each levels were calculated (Fig. 2). The average value of each

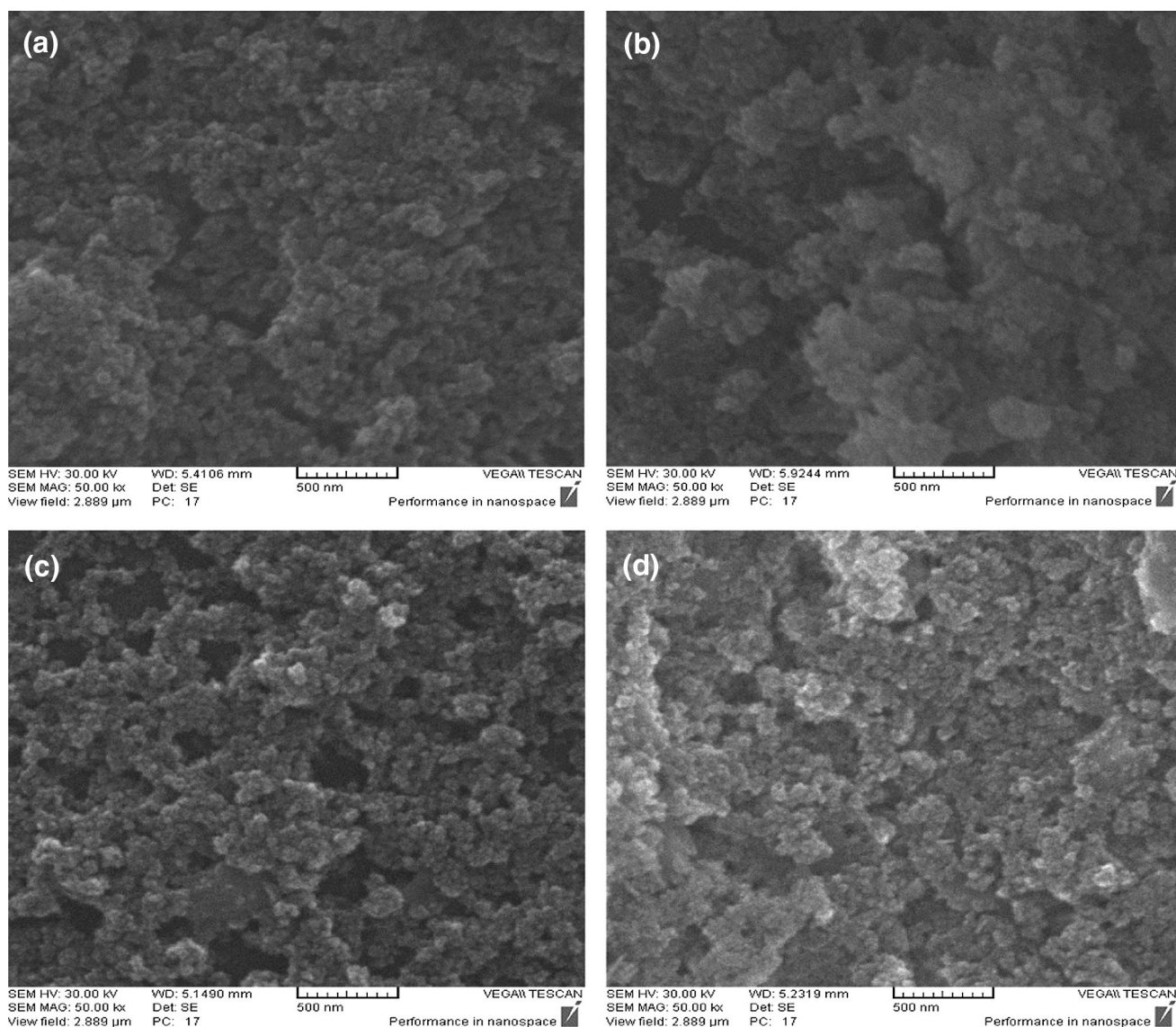


Fig. 1 SEM images of europium carbonate superstructures obtained at different runs, presented in Table 1, by carbonation reaction according to experimental conditions of: **a** run 2, **b** run 4, **c** run 7 and **d** run 8

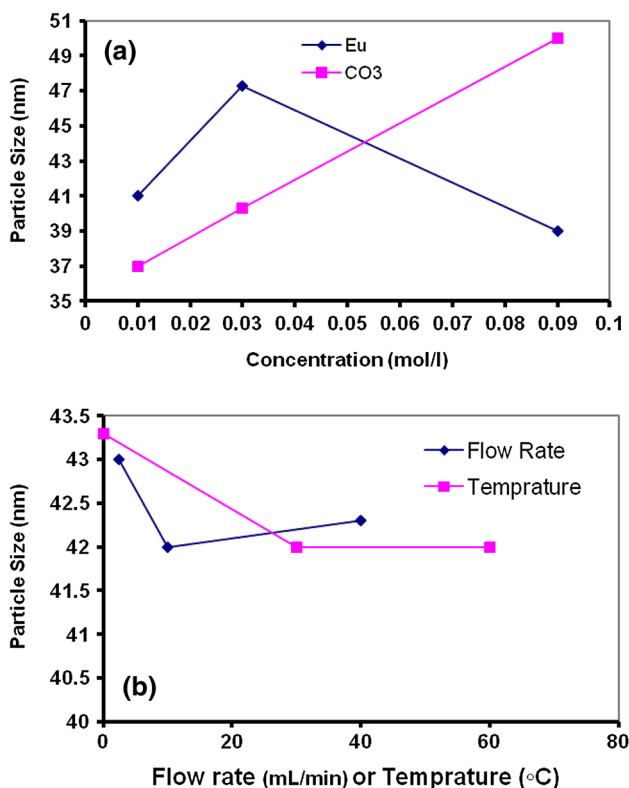


Fig. 2 Average effects for each variable at various levels **a** europium and carbonate concentration, **b** Flow rate and temperature on the size of europium carbonate nanoparticles

level of the factors is indicative of the effect of each factor on the size of the product upon varying the level.

The analysis of variance (ANOVA) was used to pinpoint the most significant factor affecting the characteristics of the product. If the variables are independent, the data analysis can help determine: (1) the optimum values for the variables, (2) the influence of each factor at different levels, as well as (3) the results of the optimum conditions (here the best dimensions of the produced precipitates) [35–38]. The results of ANOVA are illustrated in Table 2, where *S* and *V* represent the sum of square of each variable (or error term), and the variance of the results for each factor, respectively.

Table 2 Results of ANOVA for europium carbonate nanoparticles synthesis using direct carbonation procedure by OA₉(3⁴) matrix

Factor	Code	DOF	S	V	Pooled ^a			
					DOF	S'	F'	P'
Europium concentration (mol/L)	Eu	2	113.6	56.8	2	113.6	44.4	28.3
Carbonate concentration (mol/L)	CO ₃	2	273.6	136.8	2	273.6	107.1	69.1
Flow rate (mL/min)	F	2	1.6	0.8	–	–	–	–
Temperature (°C)	T	2	3.6	1.8	–	–	–	–
Error	E	–	–	–	4	5.1	–	2.6

The critical value was at 90% confidence level; pooled error results from pooling of insignificant effect

^aPercentage of contribution

Further, the significance of the control factors on the particle size, i.e. the extent at which they influence the characteristics, which can be determined based on the *F* values of the *F*-distribution, can be achieved using ANOVA results. *F* can be used for the determination of whether or not a control factor can be pooled to an error term. The experimental results commonly have a slight degree of freedom they were pooled decrease the error.

The impact of Eu³⁺ and CO₃²⁻ concentrations on the size of the synthesized europium(III) carbonate at 0.01, 0.03 and 0.09 mol/L, was studied and the results revealed that both of these values substantially influence the determination of the dimensions of the product. The effect of three different reactor temperatures, i.e. 0, 30 and 60 °C, as well as the impact of the flow rate at which the Eu³⁺ solution is added to the CO₃²⁻ solution, on the size of the product particles were also monitored. Studies revealed that neither the reactor temperature nor the flow rate had a significant influence on the particle properties.

So it was evident that at a 90% level of confidence, based on the ANOVA results, although the concentration of both ionic ingredients are significantly important, the flow rate and temperature do not leave significant effects on the properties of the product. The optimum concentrations of Eu³⁺ and CO₃²⁻ solutions, achieved through the ANOVA results, were determined to be 0.09 and 0.01 mol/L respectively.

The particle size of the product (which is regarded as the indicator of the performance of the method) under the optimal significance levels of the factors, obtained from the OA₉ (3⁴) matrix (Table 2), can be calculated according to the following expression [39, 40]:

$$Y_{opt} = \frac{T}{N} + \left(C_{Tb} - \frac{T}{N} \right) + \left(C_{CO_3} - \frac{T}{N} \right)$$

in which *T/N* represents the average size of the product particles obtained from nine experimental runs; *T* is the grand total of all particle size results, *N* is the sum of all results, *Y_{opt}* is the diameter of the product prepared using optimum Eu³⁺ and CO₃²⁻ concentrations.

The confidence interval (CI), for the particle size prepared under the optimum conditions, is calculated using the following equation [41–43]:

$$CI = \pm \sqrt{\frac{F_{\alpha}(f_1, f_2) V_e}{N_e}}$$

where $F_{\alpha}(f_1, f_2)$ represents the F value from the F table at f_1 and f_2 degrees of freedom (DOF) at the level of significance α ($\alpha=90\%$, here) and $f_1 = DOF$ of mean while and always equals 1, $f_2 = DOF$ of the error term after pooling, N_e = number of the effective replications, while is given by $N_e = \text{number of the trials}/(\text{DOF of mean (always equals 1)} + \text{total DOF of the utilized factors in the estimation})$. The product size calculated for optimal conditions and CI, at a 90% confidence level, were 33.6 ± 2.5 nm.

Run seven in Table 1 includes the optimum reaction conditions obtained from the results of ANOVA (i.e. 0.09 mol/L for Eu^{3+} and 0.01 mol/L for CO_3^{2-} concentrations). The acquired SEM images proved that the products obtained under these conditions (i.e. run 7) have an average diameter of about 33 nm (Fig. 1c) which is very well constant with the calculated results.

The results of the TEM analysis of the same product samples (Fig. 3) further confirmed their size and morphology of the product, indicating the particles to be spherical and proving their average diameter to be about 33 nm. The particles prepared under the experimental conditions of run 7 were further characterized through XRD, FT-IR and thermal analyses.

3.2 Infrared and thermal characterization of the optimal products

Given the potentials of FT-IR spectroscopy in clarifying the nature of the functional groups present in molecule, the technique was applied to the characterization of the

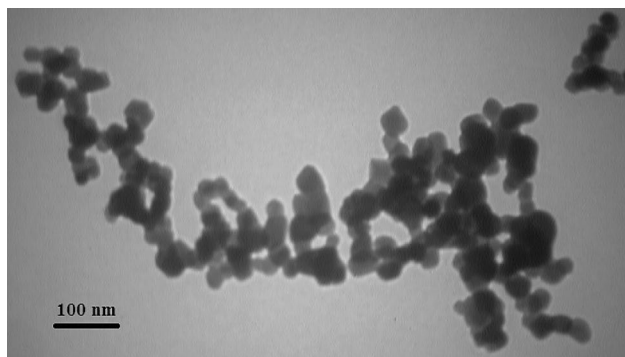


Fig. 3 TEM image of europium(III) carbonate nanoparticles obtained under optimum conditions (Run 7)

product. A typical IR spectrum of the dried optimal product is shown in Fig. 4, where the peak at 3421.1 cm^{-1} corresponds to the stretching and bending vibrations of O–H and H–O–H of the water molecules, absorbed on the surface of the dried sample during its handling to acquire the IR spectra [35, 36]. The bands at 1499.2 and 1400.7 cm^{-1} also correspond to the ν_3 mode of the carbonate group, which is split due to the inhomogeneity of the locations of the carbonate ions in the crystal structure of the product [35]. Additional bands at 1077 , 842.5 , 751.8 and 699.7 cm^{-1} can also be assigned to the ν_2 , ν_8 , ν_3 and ν_6 modes of CO_3^{2-} , respectively [44].

The thermal stability of organic and inorganic compounds are usually investigated by TG, DSC, and DTA analyses [45]. Thus, the optimal product was also analyzed through thermoanalytical techniques and the results are presented in Fig. 5.

Results of DTG-DTA performed under an inert atmosphere (nitrogen), indicated that europium carbonate samples demonstrate three mass-loss stages. The initial stage happens in the range of 50 to $150 \text{ }^\circ\text{C}$, due to the desorption of the surface absorbed water. A next weight loss phenomenon was observed between 200 and $500 \text{ }^\circ\text{C}$, and is caused by the loss of OH^- and CO_3^{2-} of the product. The third and last weight loss was observed from 520 to $600 \text{ }^\circ\text{C}$, which was most probably due to the loss of the residual carbonate species and complete decomposition of europium carbonate to Eu_2O_3 .

The thermogravimetric curves show the total mass-loss in the whole temperature range (i.e. 50 – $600 \text{ }^\circ\text{C}$), which corresponds to the desorption of water and thermal decomposition of $\text{Eu}_2(\text{CO}_3)_3$ and reach about 28% of the sample weight. Above a maximum temperature (i.e. $600 \text{ }^\circ\text{C}$) the weight of the sample was almost fixed, which can be proof that all europium carbonate present in the had is converted to Eu_2O_3 . Hence, $650 \text{ }^\circ\text{C}$ was chosen as the optimum calcination temperature.

3.3 Preparation of Eu_2O_3 from europium(III) carbonate

Based on the DTG-DTA results, the optimum products were used for the preparation of Eu_2O_3 . To this end, europium(III) carbonate was calcinated at $650 \text{ }^\circ\text{C}$ to undergo complete thermal decomposition. The scanning electron microscopy (SEM) and transmission electron microscopy (TEM) images of the product of the thermal decomposition reaction, as illustrated in Fig. 6a, b respectively, reveal and confirm the average particle size of the europium oxide to be around 60 nm (Fig. 6b).

The XRD pattern of the oxide samples presented in Fig. 7, show a strong intensity peaks and a smoothed baseline which indicates that Eu_2O_3 to have a high-purity crystalline

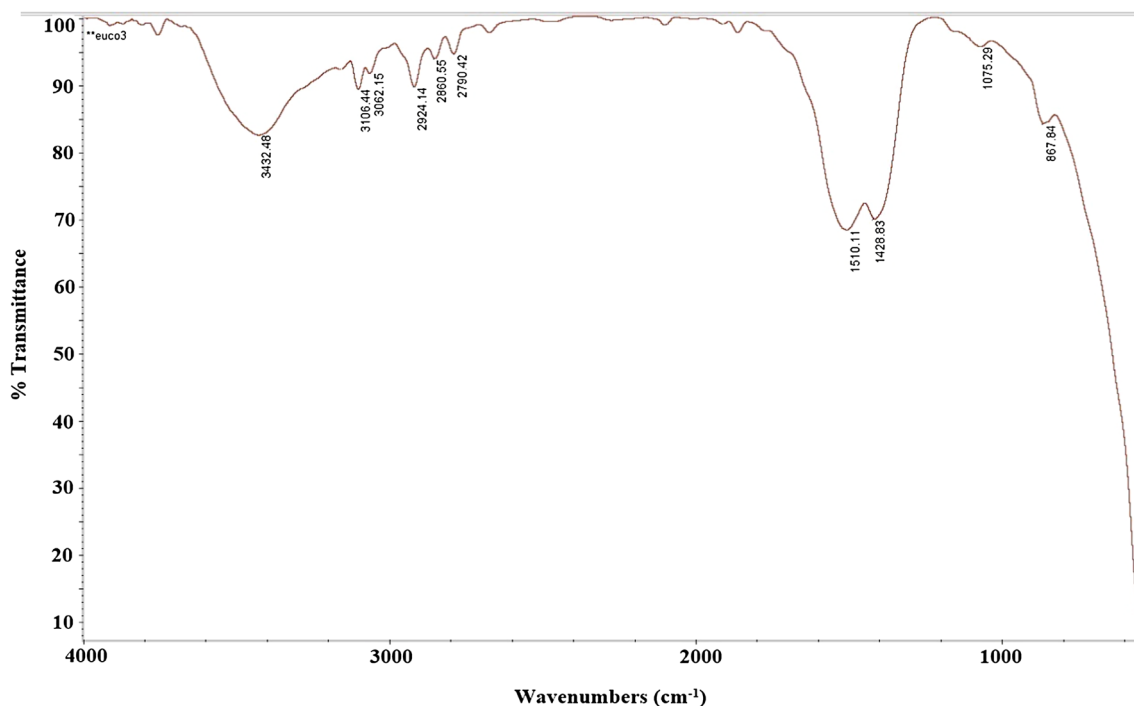
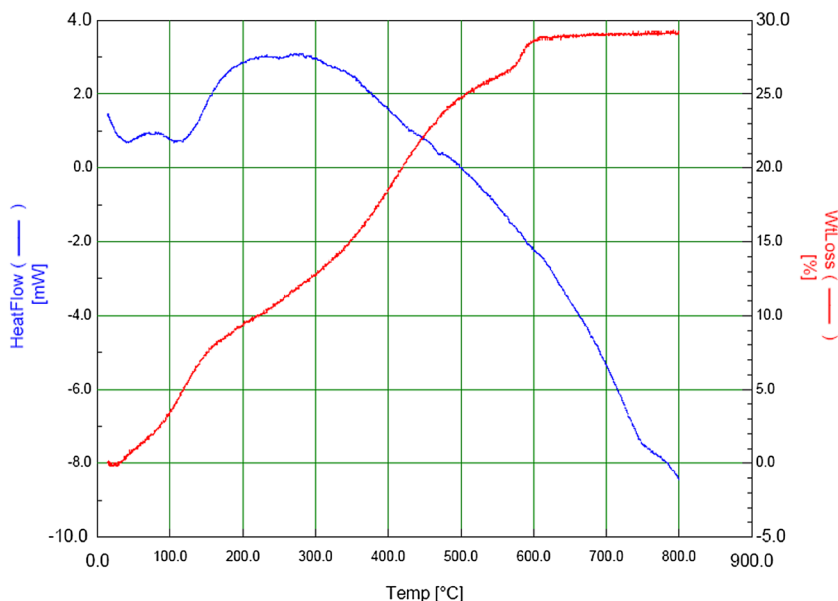


Fig. 4 FT-IR spectrum of the precipitated europium carbonate nanoparticles obtained under optimum conditions (Run 7)

Fig. 5 DTG/DTA curves for thermal decomposition reaction of europium carbonate (sample no. 7) precursor; sample mass 5.0 mg; heating rate 5 °C min⁻¹; nitrogen atmosphere. (Color figure online)



structure. All the diffraction peaks are very well consistent with the cubic system from the PDF card 01-074-1988. The average particle size of the product was determined by the Scherrer equation:

$$D = \frac{0.9 \lambda}{\beta \cos \theta}$$

where, λ is the wavelength of the X-ray radiation; $K\alpha$ for Cu is 1.5418 Å; θ represents the peak position angle; and β is the width of the observed diffraction line at half of its maximum intensity. It was concluded that the average particle size of the produced Eu_2O_3 samples ranges from 40 to 70 nm, which agrees with the SEM results.

The IR spectrum of the Eu_2O_3 samples (Fig. 8) obtained for samples prepared by the calcination of europium

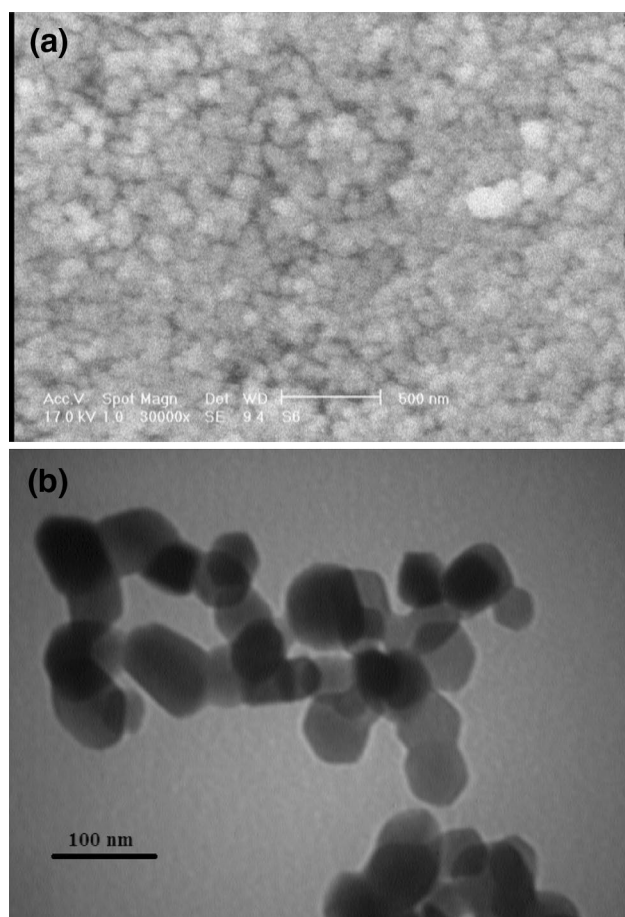
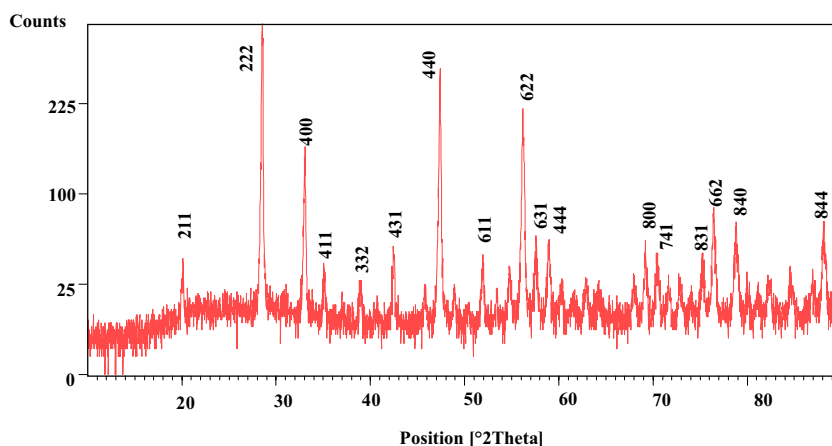


Fig. 6 **a** SEM image and **b** TEM image of europium oxide nanoparticles obtained from thermal decomposition reaction of precursor

carbonate at 650 °C for 3 h, were in consistence with previous observations [46, 47] and proved the formation of highly pure europium oxide. Comparing the IR spectra of the Eu_2O_3 with that of the precursor, i.e. europium carbonate (Fig. 4), it is evident that the peaks in the range of 3380–3600 cm^{-1} corresponding to the stretching vibrations

Fig. 7 XRD pattern of the europium oxide prepared by thermal decomposition reaction of precursor



of hydrogen bonds between the abundant hydroxyl groups in the precursor, significantly reduces in Fig. 8. This is another indication of the changes in the structure of the precursor after decomposition. The sharp peaks between 700–1000 cm^{-1} that are observed in Fig. 8 also weaken greatly and finally reach to weak fluctuations. It is noticeable that the peaks at 1383 and 1505 cm^{-1} not only weaken but also split into three absorption peaks. Also, the three peaks around 700–1100 cm^{-1} further weaken as a result of the decomposition of europium hydroxy carbonate [35, 48].

3.4 Diffuse reflectance spectroscopy (DRS)

Figure 9a, b illustrate the UV–Vis DRS results for the nanoparticles, and Fig. 10a, b present Tauc's plots for the same. The plots show the estimated band gaps of the species to be around 3.9 and 3.75 eV which correspond to absorption edge values of about 318 and 331 nm for EuCO_3 and Eu_2O_3 .

3.5 Photo-degradation reaction

Figure 11 illustrates the photocatalytic activities of optimal nanoscale EuCO_3 and Eu_2O_3 particles and Fig. 12 illustrates the concentration change behavior for the aqueous MO solution in the presence of the two nano-structures as plots of C/C_0 and degradation efficiency over irradiation time. These prove the catalytic effects of europium carbonate and europium oxide nanoparticles in the MO photo-degradation reaction. The maximum conversions (i.e. 98 and 99.3%) were observed for europium carbonate and europium oxide after 50 min.

Pseudo first-order kinetic behaviors can be observed in the plot of MO degradation over time in the presence of nano-sized EuCO_3 and Eu_2O_3 (Fig. 13). The plot of $-\ln(C/C_0)$ versus irradiation time was drawn and the slope of the linear regression was used as the 1st order reaction rate constant. This data, as well as the maximum conversions

Fig. 8 FT-IR spectrum of the europium oxide nanoparticles obtained by thermal decomposition reaction of precursor

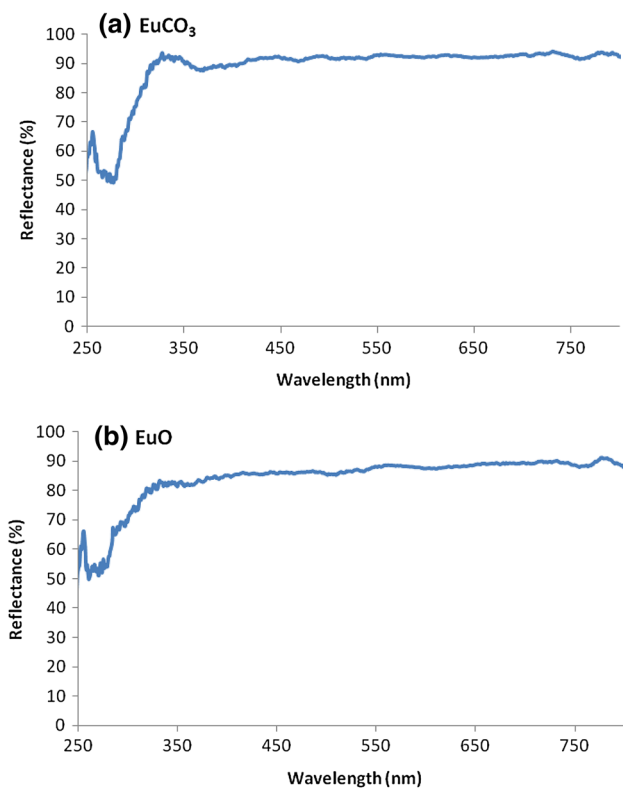
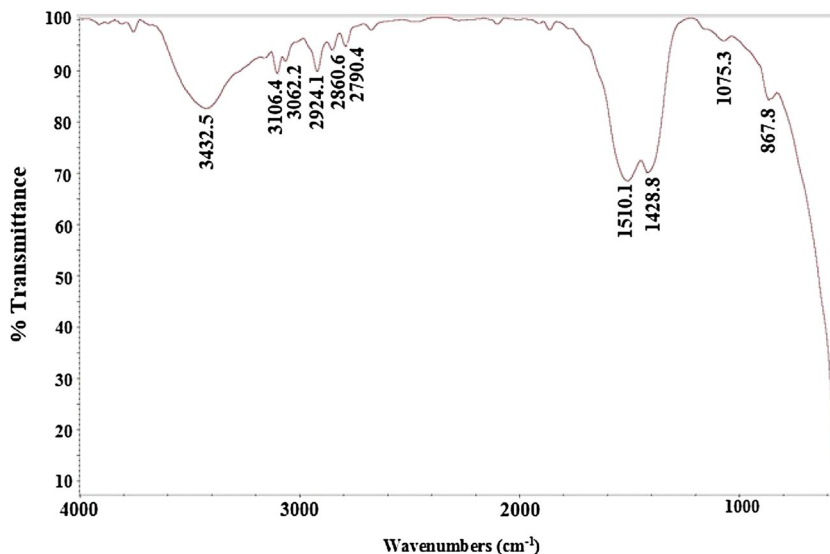


Fig. 9 UV-Vis DRS of **a** europium carbonate (europium(III) carbonate, Run 7), and **b** europium oxide (Eu_2O_3) nanoparticles

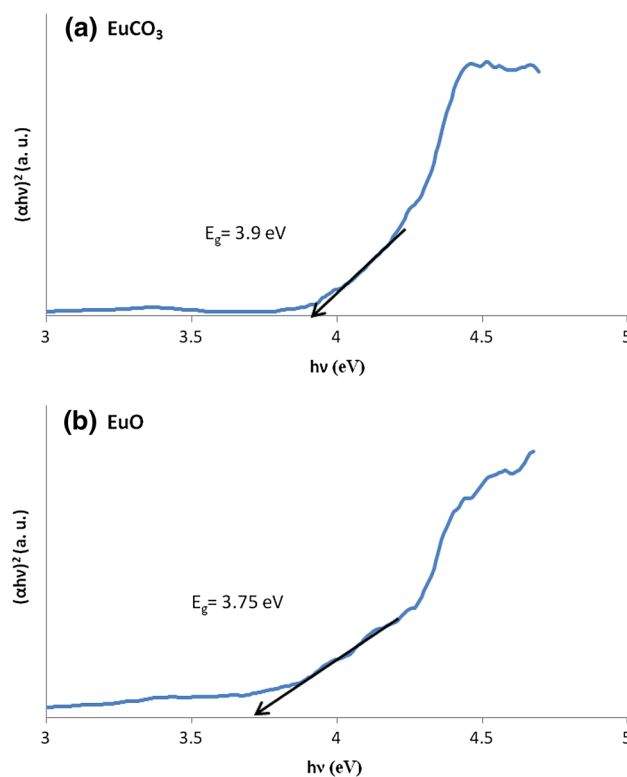


Fig. 10 Tauc's plot for **a** europium(III) carbonate (Run 7) and **b** Eu_2O_3 nanoparticles

of the photo-catalyst are given in Table 3, which proves europium carbonate and oxide nano-structures as possessing good photo-degradation abilities toward MO. This makes the nano-structures, promising candidates for photo-catalytic purification of water from this and other similar organic pollutant.

4 Conclusion

An optimized precipitation reaction has been proposed for the synthesis of the $\text{Eu}_2(\text{CO}_3)_3$ nanoparticles. The method was found to be is very controllable and suitable for the facile production of the product at low temperatures. The

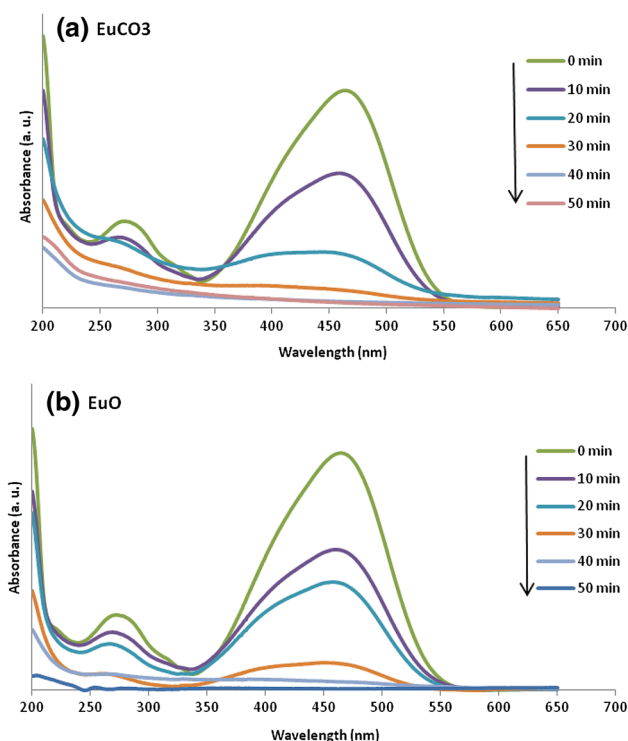


Fig. 11 UV–Vis absorbance spectra MO concentration at different irradiation times in the presence of 0.1 g/L of **a** europium(III) carbonate (Run 7), and **b** Eu_2O_3 nanoparticles as the photocatalyst

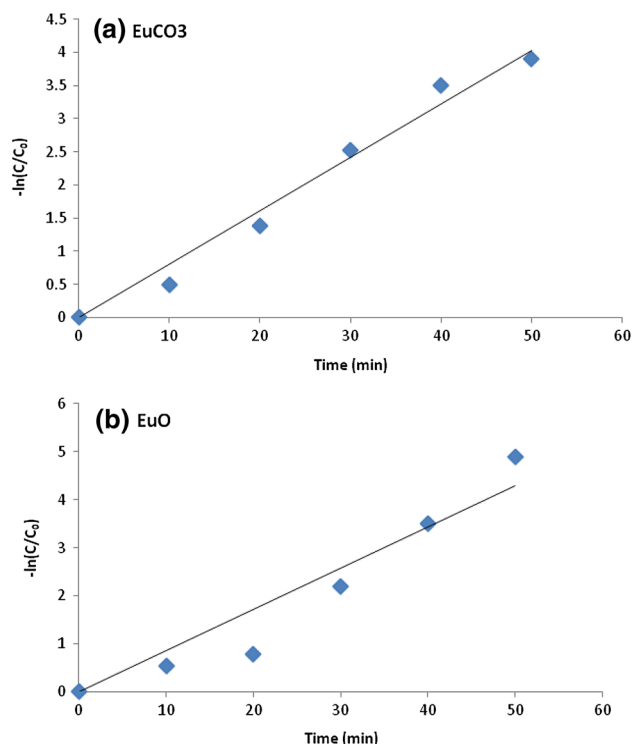


Fig. 13 Pseudo 1st order kinetics of MO degradation in the presence of **a** europium(III) carbonate (Run 7), and **b** Eu_2O_3 nanoparticles

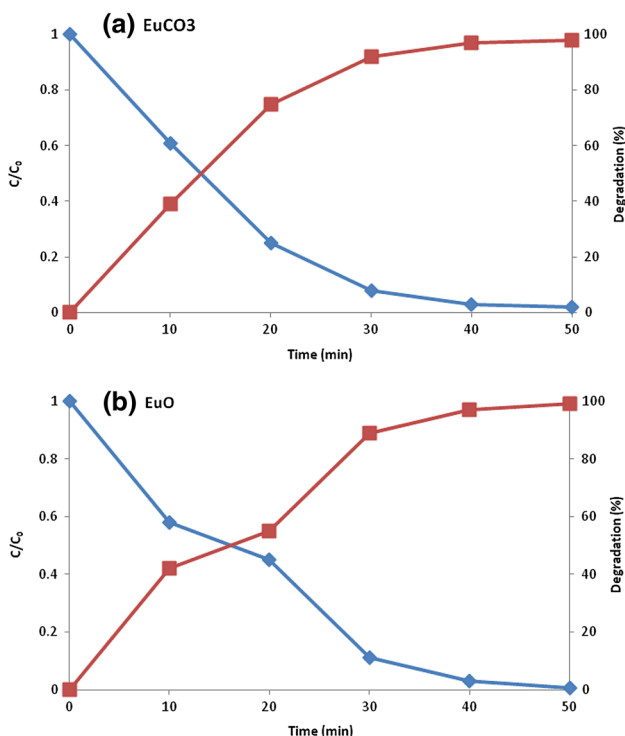


Fig. 12 Photocatalytic degradation of MO under UV irradiation using, **a** europium(III) carbonate (Run 7), and **b** Eu_2O_3 nanoparticles

Table 3 Pseudo 1st order reaction rate constants and conversion efficiencies of the particles at 50 min

Compound	K (min^{-1})	Conversion (%)
Europium carbonate	0.0806	98
Europium oxide	0.0859	99.3

optimization of the method was achieved through the Taguchi robust design for obtaining the desired particle dimensions. The results of the optimization process showed that the concentrations of the Eu^{3+} and CO_3^{2-} are very definitive in the determination of the product dimensions, while the addition flow rate and reaction temperature do not play a significant role in this regard. $\text{Eu}_2(\text{CO}_3)_3$ nanoparticles synthesized under the best conditions were found to have a diameter of about 33 nm.

Based on the results of the thermal analyses, which showed a three stage decomposition pattern for $\text{Eu}_2(\text{CO}_3)_3$, it was used as the precursor for the preparation of nanocrystalline Eu_2O_3 with average particle diameters ranging around 60 nm. Meantime, exploring the photo-catalytic behaviors of the prepared nanoparticles revealed that they both have good photo-catalytic activities and using them as photocatalysts could help reach degradation yields of about 98 and 99.3% for MO after 50 min of UV irradiation.

Acknowledgements The authors are gratefully acknowledge the financial support provided by the Iran National Science Foundation (Project 94019559).

References

- M. Rahimi-Nasrabadi, F. Ahmadi, A. Fosooni, *J. Mater. Sci.* **28**, 537 (2017)
- M. Rahimi-Nasrabadi, M. Behpour, A. Sobhani-Nasab, S.M. Hosseinpour-Mashkani, *J. Mater. Sci.* **26**, 9776 (2015)
- M. Rahimi-Nasrabadi, *J. Mater. Sci.* **28**, 2200 (2017)
- M. Rahimi-Nasrabadi, M.M. Zahedi, S.M. Pourmortazavi, J. Jazayeri, *Microchim. Acta* **177**, 145 (2012)
- M. Pirhashemi, A. Habibi-Yangjeh, *Solid State Sci.* **55**, 58 (2016)
- M. Rahimi-Nasrabadi, F. Ahmadi, M. Eghbali-Arani, *J. Mater. Sci.* **28**, 2415 (2017)
- M. Pirhashemi, A. Habibi-Yangjeh, *J. Mater. Sci.* **27**, 4098 (2016)
- M. Pirhashemi, A. Habibi-Yangjeh, *J. Colloid Interface Sci.* **474**, 103 (2016)
- M.R. Ganjali, M.B. Gholivand, M. Rahimi-Nasrabadi, B. Maddah, M. Salavati-Niasari, F. Ahmadi, *Sens. Lett.* **4**, 356 (2006).
- H.P. Yang, D.S. Zhang, L.Y. Shi, J.H. Fang, *Acta Mater.* **56**, 955 (2008)
- M. Rahimi-Nasrabadi, H.R. Naderi, M. Sadeghpour Karimi, F. Ahmadi, S.M. Pourmortazavi, *J. Mater. Sci.* **28**, 1877 (2017)
- Z. Liu, J. Zhang, R. Han, J. Du, T. Mu, Y. Wang, Z. Sun, *Microporous Mesoporous Mater.* **81**, 169 (2005)
- N. Vu, T.K. Anh, G.C. Yi, W. Strek, *J. Lumin.* **122–123**, 776 (2007)
- J.C.G. Bünzli, in *Lanthanide Probes in Life, Chemical and Earths Sciences: Theory and Practice*, ed. by J.C.G. Bünzli, G.R. Choppin (Elsevier, Amsterdam, 1989)
- Z. Xu, Y. Li, Z. Liu, Z. Xiong, *Mater. Sci. Eng. B* **110**, 302 (2004)
- B. Grobelna, B. Lipowska, A.M. Klonkowski, *J. Alloys Compd.* **419**, 191 (2006)
- A.A. Dakhel, *Eur. Phys. J. Appl. Phys.* **28**, 59–64 (2004)
- N. Vu, T.K. Anh, G.C. Yi, W. Strek, *J. Lumin.* **122**, 776 (2007)
- C.L. Chen, X.K. Wang, M. Nagatsv, *Environ. Sci. Technol.* **43**, 2362 (2009)
- T.L.R. Hower, E.C.C. Souza, T.S. Martins, E.N.S. Muccillo, R.S. Freire, *J. Mol. Catal. A* **336**, 58 (2011)
- Y.H. Xu, C. Chen, X.L. Yang, X. Li, B.F. Wang, *Appl. Surf. Sci.* **255**, 8624 (2009)
- N. Ichianose, *Superfine Particle Technology*, (Springer, Berlin, 1992)
- V.G. Pol, O. Palchik, A. Gedanken, I. Felner, *J. Phys. Chem. B* **106**, 9737 (2002)
- G. Wakefield, H.A. Keron, P.J. Dobson, J.L. Hutchison, *J. Colloid Interface Sci.* **215**, 179 (1999)
- H. Yang, D. Zhang, L. Shi, J. Fang, *Acta Mater.* **56**, 955 (2008)
- Z. Mo, Z. Deng, R. Guo, Q. Fu, C. Feng, P. Liu, Y. Sun, *Mater. Sci. Eng. B* **177**, 121 (2012).
- M. Rahimi-Nasrabadi, S.M. Pourmortazavi, M.R. Ganjali, A.R. Banan, F. Ahmadi, *J. Mol. Struct.* **1074**, 85 (2014)
- M. Rahimi-Nasrabadi, S.M. Pourmortazavi, M.R. Ganjali, P. Norouzi, F. Faridbod, M. Sadeghpour Karimi, *J. Mater. Sci.* **27**, 12860 (2016)
- M. Rahimi-Nasrabadi, S.M. Pourmortazavi, M. Aghazadeh, M.R. Ganjali, M. Sadeghpour Karimi, P. Novrouzi, *J. Mater. Sci.* **28**, 3780 (2017).
- S.M. Pourmortazavi, M. Taghdiri, N. Samimi, M. Rahimi-Nasrabadi, *Mater. Lett.* **121**, 5 (2014)
- K. Adib, M. Rahimi-Nasrabadi, Z. Rezvani, S.M. Pourmortazavi, F. Ahmadi, H.R. Naderi, M.R. Ganjali, *J. Mater. Sci.* **27**, 4541 (2016)
- M. Rahimi-Nasrabadi, F. Ahmadi, S. Hamdi, N. Eslami, K. Didehban, M.R. Ganjali, *J. Mol. Liquids* **216**, 814 (2016)
- M. Rahimi-Nasrabadi, F. Ahmadi, M. Eghbali-Arani, *J. Mater. Sci.* **27**, 11873 (2016)
- M. Rahimi-Nasrabadi, S.M. Pourmortazavi, M. Khalilian-Shalamzari, *J. Mol. Struct.* **1083**, 229 (2015)
- M. Rahimi-Nasrabadi, S.M. Pourmortazavi, M.R. Ganjali, P. Novrouzi, F. Faridbod, M. Sadeghpour Karimi, *J. Mater. Sci.* **28**, 3325 (2017)
- M. Rahimi-Nasrabadi, S.M. Pourmortazavi, M. Aghazadeh, M.R. Ganjali, M. Sadeghpour Karimi, P. Novrouzi, *J. Mater. Sci.* (2016). doi:10.1007/s10854-016-6224-4
- M. Rahimi-Nasrabadi, M.B. Gholivand, A.R. Vatanara, H. Batooli, *J. Herbs Spices Med. Plants* **18**, 318 (2012)
- S.M. Pourmortazavi, M. Rahimi-Nasrabadi, Y. Fazli, M. Mohammad-Zadeh, *Int. J. Refract. Met. Hard Mater* **51**, 29 (2015)
- S.M. Pourmortazavi, M. Rahimi-Nasrabadi, S.S. Hajimirsadeghi, *J. Dispers. Sci. Technol.* **33**, 254 (2012)
- M. Shamsipur, S.M. Pourmortazavi, S.S. Hajimirsadeghi, M.M. Zahedi, M. Rahimi-Nasrabadi, *Ceram. Int.* **39**, 819 (2013)
- S.M. Pourmortazavi, S.S. Hajimirsadeghi, M. Rahimi-Nasrabadi, I. Koksari, *Chemistry* **42**, 746 (2012)
- M. Rahimi-Nasrabadi, S.M. Pourmortazavi, M. Khalilian-Shalamzari, S.S. Hajimirsadeghi, M.M. Zahedi, *Open Chem.* **11**, 1393 (2013)
- M. Rahimi-Nasrabadi, S.M. Pourmortazavi, S.A.S. Shandiz, F. Ahmadi, H. Batooli, *Nat. Prod. Res.* **28**, 1964 (2014)
- L. Song, M. Rongjun, *J. Cryst. Growth* **169**, 190 (1996)
- S.M. Pourmortazavi, M. Rahimi-Nasrabadi, I. Koksari, S.S. Hajimirsadeghi, *J. Therm. Anal. Calorim.* **110**, 857 (2012)
- M. Rahimi-Nasrabadi, S.M. Pourmortazavi, M. Aghazadeh, M.R. Ganjali, M. Sadeghpour Karimi, P. Novrouzi, *J. Mater. Sci. Mater. Electron.* **28**, 5574 (2017)
- M. Rahimi-Nasrabadi, S. M. Pourmortazavi, M. Aghazadeh, M. R. Ganjali, *J. Mater. Sci. Mater. Electron.* (2017). doi:10.1007/s10854-017-6691-2
- M. Chandrasekhar, D.V. Sunitha, N. Dhananjaya, H. Nagabhushana, S.C. Sharma, B.M. Nagabhushana, C. Shivakumara, R.P.S. Chakradhar, *J. Lumin.* **132**, 1798 (2012)